Monodisperse MFe$_2$O$_4$ (M = Fe, Co, Mn) Nanoparticles

Shouheng Sun,*,† Hao Zeng,† David B. Robinson,† Simone Raoux,‡ Philip M. Rice,‡
Shan X. Wang,§ and Guanxiong Li§

*Contribution from the IBM T. J. Watson Research Center, Yorktown Heights, New York 10598,
IBM Almaden Research Center, 650 Harry Road, San Jose, California 95120, and Department
of Materials Science and Engineering, Stanford University, Stanford, California 94305*

Received August 22, 2003; E-mail: ssun@us.ibm.com

Abstract: High-temperature solution phase reaction of iron(III) acetylacetonate, Fe(acac)$_3$, with 1,2-hexadecanediol in the presence of oleic acid and oleylamine leads to monodisperse magnetite (Fe$_3$O$_4$) nanoparticles. Similarly, reaction of Fe(acac)$_3$ and Co(acac)$_2$ or Mn(acac)$_2$ with the same diol results in monodisperse CoFe$_2$O$_4$ or MnFe$_2$O$_4$ nanoparticles. Particle diameter can be tuned from 3 to 20 nm by varying reaction conditions or by seed-mediated growth. The as-synthesized iron oxide nanoparticles have a cubic spinel structure as characterized by HRTEM, SAED, and XRD. Further, Fe$_3$O$_4$ can be oxidized to Fe$_2$O$_3$, as evidenced by XRD, NEXAFS spectroscopy, and SQUID magnetometry. The hydrophobic nanoparticles can be transformed into hydrophilic ones by adding bipolar surfactants, and aqueous nanoparticle dispersion is readily made. These iron oxide nanoparticles and their dispersions in various media have great potential in magnetic nanodevice and biomagnetic applications.

Introduction

Magnetic iron oxide nanoparticles and their dispersions in various media have long been of scientific and technological interest. The cubic spinel structured MFe$_2$O$_4$, or MO·Fe$_2$O$_3$, represents a well-known and important class of iron oxide materials where oxygen forms an fcc close packing, and M^{2+} and Fe^{3+} occupy either tetrahedral or octahedral interstitial sites.[1] By adjusting the chemical identity of M^{2+}, the magnetic configurations of MFe$_2$O$_4$ can be molecularly engineered to provide a wide range of magnetic properties. Due in part to this versatility, nanometer-scale MFe$_2$O$_4$ materials have been among the most frequently chosen systems for studies of nanomagnetism and have shown great potential for many important technological applications, ranging from information storage and electronic devices to medical diagnostics and drug delivery. Dispersions of magnetic MFe$_2$O$_4$ nanoparticles, especially magnetite (Fe$_3$O$_4$) nanoparticles, have been used widely not only as ferrofluids in sealing, oscillation damping, and position sensing[2] but also as promising candidates for biomolecule tagging, imaging, sensing, and separation.[3] Depending on the chemical identity of M^{2+}, the densely packed solid state form of nanocrystalline MFe$_2$O$_4$-based materials, on the other hand, can have either high magnetic permeability and electrical resistivity (for M representing one or the mixed components from Co, Li, Ni, Zn, etc.) or half-metallicity (for M = Fe), and

may be a potential candidate for future high-performance electromagnetic[4] and spintronic devices.[5]

To use MFe$_2$O$_4$ nanoparticles for future highly sensitive magnetic nanodevice and biomedical applications, a practical route to monodisperse MFe$_2$O$_4$ nanoparticles with diameters smaller than 20 nm and a tight size distribution (less than 10% standard deviation) is needed. A commonly used solution phase procedure for making such particles has been the coprecipitation of M^{2+} and Fe^{3+} ions by a base, usually NaOH or NH$_3$·H$_2$O in an aqueous solution[6] or in a reverse micelle template.[7] Although this precipitation method is suitable for mass production of

---

† IBM T. J. Watson Research Center.
‡ IBM Almaden Research Center.
§ Stanford University.
(1) (a) West, A. R. *Basic Solid State Chemistry*; John Wiley & Sons: New York, 1988; pp 356−359. (b) O'Handley, R. C. *Modern Magnetic Materials−Principles and Applications*; John Wiley & Sons: New York, 2000; pp 126−132.
(2) Raj, K.; Moskowitz, R. *J. Magn. Magn. Mater.* **1990**, *85*, 233.

(3) (a) Häfeli, U.; Schütt, W.; Teller, J.; Zborowski, M. *Scientific and Clinical Applications of Magnetic Carriers*; Plenum Press: New York, 1997. (b) Oswald, P.; Clement, O.; Chambon, C.; Schouman-Claeys, E.; Frija, G. *Magn. Reson. Imaging* **1997**, *15*, 1025. (c) Hergt, R.; Andra, W.; d'Ambly, C. G.; Hilger, I.; Kaiser, W. A.; Richter, U.; Schmidt, H.-G. *IEEE Trans. Mag.* **1998**, *34*, 3745. (d) Jordan, A.; Scholz, R.; Wust, P.; Fähling, H.; Felix, R. J. *J. Magn. Magn. Mater.* **1999**, *201*, 413. (e) Kim, D. K.; Zhang, Y.; Kehr, J.; Klason, T.; Bjelke, B.; Muhammed. M. *J. Magn. Magn. Mater.* **2001**, *225*, 256. (f) Pankhurst, Q. A.; Connolly, J.; Dobson, J. *J. Phys. D: Appl. Phys.* **2003**, *36*, R167. (g) Tartaj, P.; Morales, M. P.; Veintemillas-Verdaguer, S.; González-Carreño, T.; Serna, C. J. *J. Phys. D: Appl. Phys.* **2003**, *36*, R182. (h) Berry, C. C.; Curtis, A. S. G. *J. Phys. D: Appl. Phys.* **2003**, *36*, R198.
(4) (a) Fannin, P. C.; Charles, S. W.; Vincent, D.; Giannitsis, A. T. *J. Magn. Magn. Mater.* **2002**, *252*, 80. (b) Matsushita, N.; Nakamura, T.; Abe, M. *IEEE Trans. Magn.* **2002**, *38*, 3111. (c) Matsushita, Chong, C. P.; Mizutani, T.; Abe, M. *J. Appl. Phys.* **2002**, *91*, 7376. (d) Nakamura, T.; Miyamoto, T.; Yamada, Y. *J. Magn. Magn. Mater.* **2003**, *256*, 340.
(5) (a) Verwey, E. J. W. *Nature* **1939**, *144*, 327. (b) Zhang, Z.; Satpathy, S. *Phys. Rev. B* **1991**, *44*, 13319. (c) Anisimov, V. I.; Elfimov, I. S.; Hamada, N.; Terakura, K. *Phys. Rev. B* **1996**, *54*, 4387. (d) Gong, G. Q.; Gupta, A.; Xiao, G.; Qian, W.; Dravid, D. P. *Phys. Rev. B* **1997**, *56*, 5096. (e) Coey, J. M. D.; Berkowitz, A. E.; Balcells, L. I.; Putris, F. F.; Parker, F. T. *Appl. Phys. Lett.* **1998**, *72*, 734. (f) Li, X. W.; Gupta, A.; Xiao, G.; Gong, G. Q. *J. Appl. Phys.* **1998**, *83*, 7049. (g) Kiyomura, T.; Maruo, Y.; Gomi M. *J. Appl. Phys.* **2000**, *88*, 4768. (h) Moore, R. G. C.; Evans, S. D.; Shen, T.; Hodson, C. E. C. *Physica E* **2001**, *9*, 253. (i) Versluijs, J. J.; Bari, M. A.; Coey, J. M. D. *Phys. Rev. Lett.* **2001**, *87*, 26601. (j) Soeya, S.; Hayakawa, J.; Takahashi, H.; Ito, K.; Yamamoto, C.; Kida, A.; Asano, H.; Matsui, M. *Appl. Phys. Lett.* **2002**, *80*, 823. (k) Sorenson, T. A.; Morton, S. A.; Dan Waddill, G.; Switzer, J. A. *J. Am. Chem. Soc.* **2002**, *124*, 7604.

---

magnetic MFe_2O_4 ferrofluids, it does require careful adjustment of the pH value of the solution for particle formation and stabilization, and it is difficult to control sizes and size distributions, particularly for particles smaller than 20 nm. An alternative approach to monodisperse iron oxide nanoparticles is via high-temperature organic phase decomposition of an iron precursor, for example, decomposition of $FeCup_3$ (Cup: *N*-nitrosophenylhydroxylamine, $C_6H_5N(NO)O^-$)[8] or decomposition of $Fe(CO)_5$ followed by oxidation to Fe_2O_3.[9] The latter process has recently been extended to the synthesis of monodisperse cobalt ferrite ($CoFe_2O_4$) nanoparticles.[10] Although significant progress in making monodisperse Fe_2O_3 and $CoFe_2O_4$ nanoparticles has been made in organic phase reactions, there is still no general process for producing MFe_2O_4, especially Fe_3O_4 nanoparticles with the desired size and acceptable size distribution.

Recently, we reported a convenient organic phase process for making monodisperse Fe_3O_4 nanoparticles through the reaction of $Fe(acac)_3$ and a long-chain alcohol.[11] Our further experiments indicated that this reaction could be readily extended to the synthesis of MFe_2O_4 nanoparticles (with M = Co, Ni, Mn, Mg, etc.) by simply adding a different metal acetylacetonate precursor to the mixture of $Fe(acac)_3$ and 1,2-hexadecanediol. Here we present detailed syntheses and characterization of Fe_3O_4 and related MFe_2O_4 nanoparticles (with M = Co and Mn as two examples) with sizes tunable from 3 to 20 nm in diameter. The process involves high-temperature (up to 305 °C) reaction of metal acetylacetonate with 1,2-hexadecanediol, oleic acid, and oleylamine. The size of the oxide nanoparticles can be controlled by varying the reaction temperature or changing metal precursors. Alternatively, with the smaller nanoparticles as seeds, larger monodisperse nanoparticles up to 20 nm in diameter can be synthesized by seed-mediated growth. The process does not require a low-yield fractionation procedure to achieve the desired size distribution and is readily scaled up for mass production. The nanoparticles can be dispersed into nonpolar or weakly polar hydrocarbon solvent, such as hexane or toluene. The hydrophobic nanoparticles can be transformed into hydrophilic ones by mixing with a bipolar surfactant, tetramethylammonium 11-aminoundecanoate, allowing preparation of aqueous nanoparticle dispersions. These iron oxide nanoparticles and their dispersions in various media have great potential in magnetic nanodevice and biomagnetic applications.

(6) See for example: (a) Kang, Y. S.; Risbud, S.; Rabolt, J. F.; Stroeve, P. *Chem. Mater*. **1996**, *8*, 2209. (b) Hong, C.-Y.; Jang, I. J.; Horng, H. E.; Hsu, C. J.; Yao, Y. D.; Yang, H. C. *J. Appl. Phys*. **1997**, *81*, 4275. (c) Fried, T.; Shemer, G.; Markovich, G. *Adv. Mater*. **2001**, *13*, 1158. (d) Tang, Z. X.; Sorensen, C. M.; Klabunde, K. J.; Hadjipanayis, G. C. *J. Colloid Interface Sci*. **1991**, *146*, 38. (e) Zhang, Z. J.; Wang, Z. L.; Chakoumakos, B. C.; Yin, J. S. *J. Am. Chem. Soc*. **1998**, *120*, 1800. (f) Neveu, S.; Bec, A.; Robineau, M.; Talbot, D. *J. Colloid Interface Sci*. **2002**, *255*, 293.
(7) See for example: (a) Pileni, M. P.; Moumen, N. *J. Phys. Chem. B* **1996**, *100*, 1867. (b) Liu, C.; Zou, B.; Rondinone, A. J.; Zhang, Z. J. *J. Phys. Chem. B* **2000**, *104*, 1141.
(8) Rockenberger, J.; Scher, E. C.; Alivisatos, P. A. *J. Am. Chem. Soc*. **1999**, *121*, 11595.
(9) (a) Bentzon, M. D.; van Wonterghem, J.; Mørup, S.; Thölén, A.; Koch, C. J. *Philos. Mag. B* **1989**, *60*, 169. (b) Hyeon, T.; Lee, S. S.; Park, J.; Chung, Y.; Na, H. B. *J. Am. Chem. Soc*. **2001**, *123*, 12798. (c) Guo, Q.; Teng, X.; Rahman, S.; Yang, H. *J. Am. Chem. Soc*. **2003**, *125*, 630. (d) Redl, F. X.; Cho, K.-S.; Murray, C. B.; O'Brien, S. *Nature* **2003**, *423*, 968.
(10) Hyeon, T.; Chung, Y.; Park, J.; Lee, S. S.; Kim, Y.-W.; Park, B. H. *J. Phys. Chem. B* **2002**, *106*, 6831.
(11) Sun, S.; Zeng, H. *J. Am. Chem. Soc*. **2002**, *124*, 8204.

Experimental Section

The synthesis was carried out using standard airless procedures and commercially available reagents. Absolute ethanol, hexane, and dichloromethane (99%) were used as received. Phenyl ether (99%), benzyl ether (99%), 1,2-hexadecanediol (97%), oleic acid (90%), oleylamine (>70%), cobalt(II) acetylacetonate, Mn(II) acetylacetonate, and polyethylenimine (water-free, average M_w ca. 25 000) were purchased from Aldrich Chemical Co. Iron(III) acetylacetonate was from Strem Chemicals, Inc. Tetramethylammonium 11-aminoundecanoate was prepared by titrating a methanolic suspension of 11-aminoundecanoic acid with methanolic tetramethylammonium hydroxide (both from Aldrich), evaporating the solvent under reduced pressure, and recrystallizing in tetrahydrofuran.

Synthesis of 4 nm Fe_3O_4 Nanoparticle Seeds. $Fe(acac)_3$ (2 mmol), 1,2-hexadecanediol (10 mmol), oleic acid (6 mmol), oleylamine (6 mmol), and phenyl ether (20 mL) were mixed and magnetically stirred under a flow of nitrogen. The mixture was heated to 200 °C for 30 min and then, under a blanket of nitrogen, heated to reflux (265 °C) for another 30 min. The black-brown mixture was cooled to room temperature by removing the heat source. Under ambient conditions, ethanol (40 mL) was added to the mixture, and a black material was precipitated and separated via centrifugation. The black product was dissolved in hexane in the presence of oleic acid (~0.05 mL) and oleylamine (~0.05 mL). Centrifugation (6000 rpm, 10 min) was applied to remove any undispersed residue. The product, 4 nm Fe_3O_4 nanoparticles, was then precipitated with ethanol, centrifuged (6000 rpm, 10 min) to remove the solvent, and redispersed into hexane.

Under identical conditions, reaction of $Co(acac)_2$ (1 mmol) with $Fe(acac)_3$ led to 3 nm $CoFe_2O_4$ nanoparticles that could be readily dispersed into hexane, giving a dark red-brown hexane dispersion.

Synthesis of 6 nm Fe_3O_4 Nanoparticle Seeds. $Fe(acac)_3$ (2 mmol), 1,2-hexadecanediol (10 mmol), oleic acid (6 mmol), oleylamine (6 mmol), and benzyl ether (20 mL) were mixed and magnetically stirred under a flow of nitrogen. The mixture was heated to 200 °C for 2 h and then, under a blanket of nitrogen, heated to reflux (~300 °C) for 1 h. The black-colored mixture was cooled to room temperature by removing the heat source. Following the workup procedures described in the synthesis of 4 nm particles, a black-brown hexane dispersion of 6 nm Fe_3O_4 nanoparticles was produced.

Similarly, by adding $Co(acac)_2$ or $Mn(acac)_2$, 10 nm $CoFe_2O_4$ or 7 nm $MnFe_2O_4$ nanoparticle seeds can be made.

Synthesis of 8 nm Fe_3O_4 Nanoparticles via 6 nm Fe_3O_4 Seeds. $Fe(acac)_3$ (2 mmol), 1,2-hexadecanediol (10 mmol), benzyl ether (20 mL), oleic acid (2 mmol), and oleylamine (2 mmol) were mixed and magnetically stirred under a flow of N_2. A 84 mg sample of 6 nm Fe_3O_4 nanoparticles dispersed in hexane (4 mL) was added. The mixture was first heated to 100 °C for 30 min to remove hexane, then to 200 °C for 1 h. Under a blanket of nitrogen, the mixture was further heated to reflux (~300 °C) for 30 min. The black-colored mixture was cooled to room temperature by removing the heat source. Following the workup procedures described in the synthesis of 4 nm particles, a black-brown hexane dispersion of 8 nm Fe_3O_4 nanoparticles was produced.

Similarly, 80 mg of 8 nm Fe_3O_4 seeds reacted with $Fe(acac)_3$ (2 mmol) and the diol (10 mmol) led to 10 nm Fe_3O_4 nanoparticles. Using this seed-mediated growth, bigger nanoparticles of Fe_3O_4 up to 20 nm, $CoFe_2O_4$ up to 20 nm, or $MnFe_2O_4$ up to 18 nm have been made.

Synthesis of Hydrophilic Fe_3O_4 Nanoparticles. Under ambient conditions, a hexane dispersion of hydrophobic Fe_3O_4 nanoparticles (about 20 mg in 0.2 mL) was added to a suspension of tetramethylammonium 11-aminoundecanoate (about 20 mg in 2 mL) in dichloromethane. The mixture was shaken for about 20 min, during which time the particles precipitated and separated using a magnet. The solvent and nonmagnetic suspension were decanted, and the precipitate was washed once with dichloromethane and separated again using a magnet

Scheme 1

Fe(acac)$_3$ + 1,2-RCH(OH)CH$_2$OH + RCOOH + RNH$_2$

⇓ solvent

⇓ 200°C

⇓ refluxing
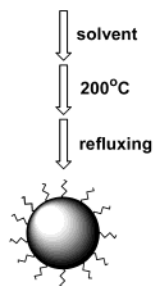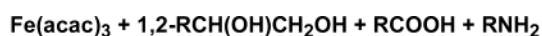
to remove excess surfactants before drying under N$_2$. The product was then dispersed in deionized water (18 MΩ) or 1 mM phosphate buffer at neutral pH.

Nanoparticle Characterization. Fe, Co, Mn, and S elemental analyses of the as-synthesized nanoparticle powders were performed on inductively coupled plasma−optic emission spectrometry (ICP-OES) at Galbraith Laboratories (Knoxville, TN). To prepare samples for elemental analysis, the particles were precipitated from their hexane dispersion by ethanol, centrifuged, washed with ethanol, and dried. Samples for transmission electron microscopy (TEM) analysis were prepared by drying a dispersion of the particles on amorphous carbon-coated copper grids. Particles were imaged using a Philips CM 12 TEM (120 kV). The structure of the particles was characterized using HRTEM and selected area electron diffraction (SAED) on a JEOL TEM (400 kV). X-ray powder diffraction patterns of the particle assemblies were collected on a Siemens D-500 diffractometer under Co Kα radiation (λ = 1.788965 Å). Near-edge X-ray absorption fine structure (NEXAFS) spectroscopy was performed at the Advanced Light Source at beamline 7.3.1.1, which was equipped with a spherical grating monochromator and had an energy resolution of $E/\Delta E$ = 1800. Magnetic studies were carried out using a MPMS2 Quantum Design SQUID magnetometer with fields up to 7 T and temperatures from 5 to 350 K. Infrared spectra of dried particles pressed into KBr pellets were obtained on a Nicolet Nexus 670 FTIR spectrometer. A homemade spin valve sensor[12] was used to detect a single layer of 16 nm Fe$_3$O$_4$ nanoparticles.

Results and Discussion

Fe$_3$O$_4$ Synthesis. As illustrated in Scheme 1, reaction of Fe-(acac)$_3$ with surfactants at high temperature leads to monodisperse Fe$_3$O$_4$ nanoparticles, which can be easily isolated from reaction byproducts and the high boiling point ether solvent. If phenyl ether was used as solvent, 4 nm Fe$_3$O$_4$ nanoparticles were separated, while the use of benzyl ether led to 6 nm Fe$_3$O$_4$. As the boiling point of benzyl ether (298 °C) is higher than that of phenyl ether (259 °C), the larger sized Fe$_3$O$_4$ particle obtained from benzyl ether solution seems to indicate that high reaction temperature will yield larger particles. However, regardless of the size of the particles, the key to the success of making monodisperse nanoparticles is to heat the mixture to 200 °C first and remain at that temperature for some time before it is heated to reflux at 265 °C in phenyl ether or at ∼300 °C in benzyl ether. Directly heating the mixture to reflux from room temperature would result in Fe$_3$O$_4$ nanoparticles with wide size distribution from 4 to 15 nm, indicating that the nucleation of Fe$_3$O$_4$ and the growth of the nuclei under these reaction conditions is not a fast process.

The low cost of Fe(acac)$_3$ and the high yields it produces makes it an ideal precursor for Fe$_3$O$_4$ nanoparticle synthesis. The more expensive Fe(acac)$_2$ or Fe(II) acetate can also be used but yields no better result than Fe(acac)$_3$. Fe(II) (D-gluconate) is another good precursor for Fe$_3$O$_4$ synthesis. In benzyl ether, the reaction of Fe(II) (D-gluconate) with a 3-fold excess of each of oleic acid and oleylamine and a 5-fold excess of 1,2-hexadecanediol led to nearly monodisperse 8 nm Fe$_3$O$_4$ nanoparticles.

Several different alcohols and polyalcohols have been tested for their reactions with Fe(acac)$_3$. It was found that 1,2-hydrocarbon diols, including 1,2-hexadecanediol and 1,2-dodecanediol, react well with Fe(acac)$_3$ to yield Fe$_3$O$_4$ nanoparticles. Long-chain monoalcohols, such as stearyl alcohol and oleyl alcohol, can also be used, but particle quality is worse and product yield is poorer than those with diols in the synthesis of Fe$_3$O$_4$ nanoparticle seeds. However, in the seed-mediated growth process, these monoalcohols can be used to form larger Fe$_3$O$_4$ nanoparticles.[11]

Oleic acid and oleylamine are necessary for the formation of particles. Sole use of oleic acid during the reaction resulted in a viscous red-brown product that was difficult to purify and characterize. On the other hand, the use of oleylamine alone produced iron oxide nanoparticles in a much lower yield than the reaction in the presence of both oleic acid and oleylamine. When the 4 nm particles were oxidized by bubbling oxygen through the dispersion at room temperature, they precipitated from hexane as a red-brown powder (the characterization of a similar product is discussed below). Adding more oleic acid did not cause re-dispersion of this powder into hexane. However, adding oleylamine did, leading to an orange-brown hexane dispersion. This is consistent with the previous observation that γ-Fe$_2$O$_3$ nanoparticles can be stabilized by alkylamine surfactants,[13] suggesting that −NH$_2$ coordinates with Fe(III) on the surface of the particles.

The larger Fe$_3$O$_4$ nanoparticles can also be made by seed-mediated growth. This method has been recently applied to larger metallic nanoparticle and nanocomposite synthesis[14] and is believed to be an alternative way of making monodisperse nanoparticles along with LaMer's method through fast super-saturated-burst nucleation[15] and Finke's method via slow, continuous nucleation and fast, autocatalytic surface growth.[16] In our synthesis, the small Fe$_3$O$_4$ nanoparticles, the seeds, are mixed with more materials as shown in Scheme 1 and heated, and particle diameters can be increased by ∼2 nm or more in each seed-mediated reaction, allowing diameter to be tuned up to about 20 nm.

TEM analysis shows that Fe$_3$O$_4$ nanoparticles prepared according to Scheme 1 or the seed-mediated growth method are monodisperse. Figure 1 shows typical TEM images from representative 6, 10, and 12 nm Fe$_3$O$_4$ nanoparticles deposited from their hexane (or octane) dispersions and dried under ambient conditions. It can be seen that the particles have a

(12) Li, G.; Joshi, V.; White, R. L.; Wang, S. X.; Kemp, J. T.; Webb, C.; Davis, R. W.; Sun, S. *J. Appl. Phys.* **2003**, *93*, 7557.

(13) (a) Rajamathi, M.; Ghosh, M.; Seshadri, R. *Chem. Comm.* **2002**, 1152. (b) Boal, A. K.; Das, K.; Gray, M.; Rotello, V. M. *Chem. Mater.* **2002**, *14*, 2628.

(14) (a) Brown, K. R.; Natan, M. J. *Langmuir* **1998**, *14*, 726. (b) Jana, N. R.; Gearheart, L.; Murphy, C. J. *Chem. Mater.* **2001**, *13*, 2313. (c) Yu, H.; Gibbons, P. C.; Kelton, K. F.; Buhro, W. E. *J. Am. Chem. Soc.* **2001**, *123*, 9198.

(15) LaMer, V. K.; Dinegar, R. H. *J. Am. Chem. Soc.* **1950**, *72*, 4847.

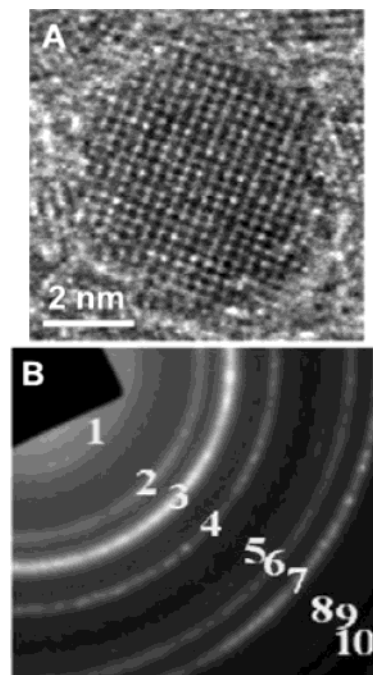(16) Watzky, M. A.; Finke, R. G. *J. Am. Chem. Soc.* **1997**, *119*, 10382.
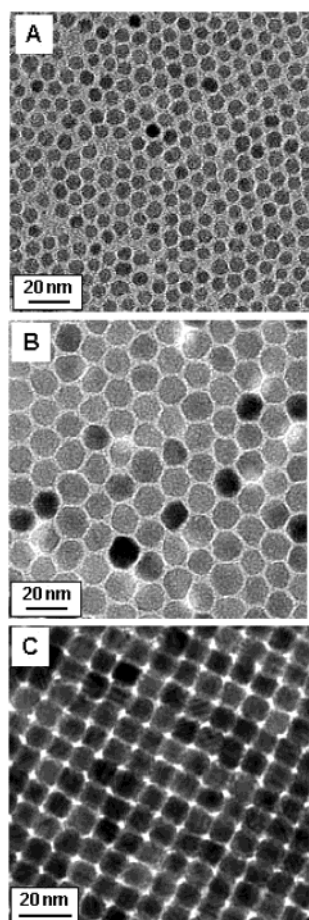
Figure 1. TEM bright field images of (A) 6 nm and (B) 12 nm Fe$_3$O$_4$ nanoparticles deposited from their hexane dispersion on an amorphous carbon-coated copper grid and dried at room temperature, and (C) a 3D superlattice of 10 nm Fe$_3$O$_4$ nanoparticles deposited from their octane dispersion on an amorphous carbon surface and dried at room temperature.

narrow size distribution and can form a self-ordered Fe$_3$O$_4$ superlattice (Figure 1C) if solvent is made to evaporate slowly.

Fe$_3$O$_4$ Structural Characterization. Structural information from a single Fe$_3$O$_4$ nanoparticle was obtained using high-resolution TEM (HRTEM). Figure 2A is the HRTEM image of an isolated 6 nm Fe$_3$O$_4$ nanoparticle. The lattice fringes in the image correspond to a group of atomic planes within the particle, indicating that the particle is a single crystal. The distance between two adjacent planes is measured to be 2.98 Å, corresponding to (220) planes in the spinel-structured Fe$_3$O$_4$.[17]

Structural information from an assembly of Fe$_3$O$_4$ nanoparticles was obtained from both electron and X-ray diffraction. Figure 2B is a selected area electron diffraction (SAED) pattern acquired from a 6 nm nanoparticle assembly. Table 1 displays the measured lattice spacing based on the rings in the diffraction pattern and compares them to the known lattice spacing for bulk Fe$_3$O$_4$ along with their respective *hkl* indexes from the PDF database. Figure 3 is a group of representative size-dependent XRD patterns of Fe$_3$O$_4$ nanoparticles. The position and relative intensity of all diffraction rings/peaks match well with standard Fe$_3$O$_4$ powder diffraction data.[17] The average particle diameter

(17) Cornell, R. M.; Schwertmann, U. *The Iron Oxides: Structure, Properties, Reactions, Occurrence and Uses*; VCH: New York, 1996; pp 167−168.

Figure 2. Structural characterization of Fe$_3$O$_4$ nanoparticles: (A) High-Resolution TEM image of a single 6 nm Fe$_3$O$_4$ nanoparticle; and (B) selected area electron diffraction (SAED) pattern acquired from a 6 nm Fe$_3$O$_4$ nanoparticle assembly.
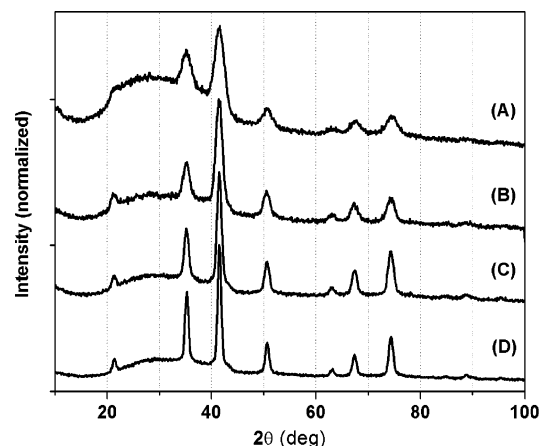
Figure 3. X-ray diffraction patterns of (A) 4 nm, (B) 8 nm, (C) 12 nm, and (D) 16 nm Fe$_3$O$_4$ nanoparticle assemblies. All samples were deposited on glass substrates from their hexane dispersions. Diffraction patterns were collected on a Siemens D-500 diffractometer under Co Kα radiation ($\lambda =$ 1.788965 Å).

Table 1. Measured Lattice Spacing, *d* (Å), Based on the Rings in Figure 2B and Standard Atomic Spacing for Fe$_3$O$_4$ along with Their Respective *hkl* Indexes from the PDF Database

	ring									
	1	2	3	4	5	6	7	8	9	10
d	4.86	2.98	2.54	2.12	1.73	1.63	1.5	1.34	1.29	1.22
Fe$_3$O$_4$	4.86	2.97	2.53	2.1	1.71	1.62	1.48	1.33	1.28	1.21
hkl	111	220	311	400	422	511	440	620	533	444

estimated from Scherrer's formula[18] is consistent with that determined by statistical analysis of the TEM images, indicating that each individual particle is a single crystal.
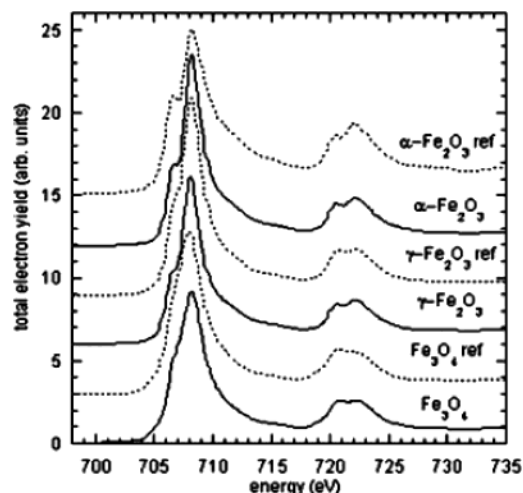
(18) Klug, H. P.; Alexander, L. E. *X-Ray Diffraction Procedures for Polycrystalline and Amorphous Materials*; John Wiley & Sons: New York, 1962; pp 491−538.
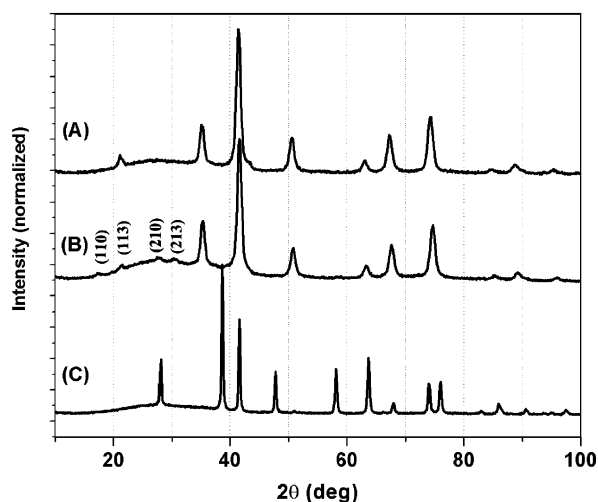
Figure 4. X-ray diffraction patterns of (A) a 16 nm Fe_3O_4 nanoparticle assembly, (B) a γ-Fe_2O_3 nanoparticle assembly obtained from the oxidation of (A) under oxygen at 250 °C for 6 h, (C) an α-Fe_2O_3 nanoparticle assembly obtained from the further annealing of (B) under Ar at 500 °C for 1 h.

Oxidation Fe_3O_4 to Fe_2O_3. It is well known that Fe_3O_4 can be oxidized to γ-Fe_2O_3, which can be further transformed into α-Fe_2O_3 at higher temperature.[19] Observation of these transformations can further help to confirm the formation of Fe_3O_4 nanoparticles from the synthesis based on Scheme 1. Figure 4A is the XRD pattern from the as-synthesized, black 16 nm Fe_3O_4 nanoparticle assembly. After oxidation under O_2 at 250 °C for 6 h, the black assembly is transformed to a red-brown one. Figure 4B shows that all XRD peak positions and relative intensities of this red-brown material match well with those of commercial γ-Fe_2O_3 powder materials (Aldrich catalog No. 48,-066-5), indicating that the oxidation of Fe_3O_4 under O_2 leads to γ-Fe_2O_3. Compared to Figure 4A, the large-angle peaks in Figure 4B shift slightly to higher angles, whereas at lower angles there exist additional weak diffraction peaks of (110), (113), (210), and (213) that are characteristic of γ-Fe_2O_3.[17] Figure 4C shows the XRD of the dark red-brown materials obtained after 500 °C annealing of γ-Fe_2O_3 in Figure 4B under Ar for 1 h. The diffraction pattern matches with that from known α-Fe_2O_3 materials,[17] indicating the transformation of γ-Fe_2O_3 to α-Fe_2O_3 at high temperature. However the as-synthesized Fe_3O_4 nanoparticles do not go through such a change if annealed under inert atmosphere. Even at 650 °C, the Fe_3O_4 structure is still retained, as evidenced by both XRD and HRTEM. This confirms the valence state of the iron cations in the as-synthesized sample closely matches that of Fe_3O_4 rather than similarly structured γ-Fe_2O_3.[20]

The transformations of Fe_3O_4 to Fe_2O_3 can be further characterized by near-edge X-ray absorption fine structure (NEXAFS) spectroscopy in total electron yield mode. Figure 5 shows the NEXAFS spectra at the Fe L absorption edges of the as-synthesized 8 nm Fe_3O_4 nanoparticles and γ-Fe_2O_3 and α-Fe_2O_3 nanoparticles derived from the oxidation of the Fe_3O_4 particles. For comparison, reference spectra of Fe_3O_4, γ-Fe_2O_3,

(19) Bate, G. In *Magnetic Oxides Part 2*; Craik, D. J., Ed.; John Wiley & Sons: New York, 1975; pp 705−707.
(20) Although the evidence presented so far suggests that Fe_3O_4 is obtained during the synthesis, one should keep in mind that the real composition of the nanoparticles may not be 100% Fe_3O_4, but contain a small amount of γ-Fe_2O_3, especially on the surface of the particles.

Figure 5. NEXAFS spectra at the Fe L edge of Fe_3O_4, γ-Fe_2O_3, and α-Fe_2O_3 nanoparticle assemblies, with the dotted lines representing reference spectra of thin film oxide samples of Fe_3O_4, γ-Fe_2O_3, and α-Fe_2O_3.
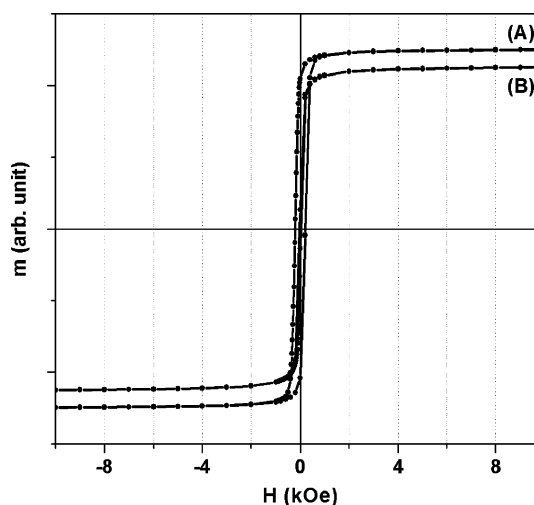
Figure 6. Hysteresis loops of the 16 nm Fe_3O_4 nanoparticle assembly measured at (A) 10 K and (B) 300 K.

and α-Fe_2O_3 films grown on MgO (001)[21] are also inserted into the figure as dotted lines. The increased splitting of the L_3 peak in the region of 705−710 eV and the varying ratio of the two peaks at the L_2 edge (719−725 eV) are indicative of the transformation of the as-synthesized Fe_3O_4 nanoparticles into γ-Fe_2O_3 and to α-Fe_2O_3 under different annealing conditions.

Magnetic Properties of the Fe_3O_4 Nanoparticle Assemblies. Magnetic measurements on all Fe_3O_4 nanoparticles indicate that the particles are superparamagnetic at room temperature, meaning that the thermal energy can overcome the anisotropy energy barrier of a single particle, and the net magnetization of the particle assemblies in the absence of an external field is zero. Figure 6 shows the hysteresis loops of 16 nm Fe_3O_4 nanoparticles measured at both 10 K and room temperature. It can be seen that the particles are ferromagnetic at 10 K with a coercivity of 450 Oe (Figure 6A). At room temperature there is no hysteresis (Figure 6B). Under a large external field, the magnetization of the particles aligns with the field direction and reaches its saturation value (saturation magnetization, σ_s). For Fe_3O_4 nanoparticles, we noticed that the

(21) Farrow, R. F.; Rice, P. M.; Toney, M. F.; Marks, R. F.; Hedstrom, J. A.; Stephenson, R.; Carey, M. J.; Kellock, A. J. *J. Appl. Phys.* **2003**, *93*, 5626.

σ_s was dependent on the size of the particles. For example, σ_s for 16 nm Fe_3O_4 nanoparticles is 83 emu/g, close to the value of 84.5 emu/g measured from the commercial magnetite fine powder. For particles smaller than 10 nm, however, σ_s is smaller, most likely due to the surface spin canting of the small magnetic nanoparticles.[22] However, if annealed under Ar at high temperature (600 °C), even 4 nm Fe_3O_4 nanoparticles show a σ_s close to 82 emu/g due to the average size increase caused by particle aggregation. After the 16 nm Fe_3O_4 nanoparticles were oxidized under oxygen at 250 °C for 6 h, their σ_s is reduced to 70 emu/g, close to 74 emu/g from commercial γ-Fe_2O_3 powder, suggesting the transformation of Fe_3O_4 to Fe_2O_3.

Possible Mechanism for the Formation of Fe_3O_4. The mechanism leading to Fe_3O_4 in the reactions presented is not yet clear. However, evidence suggests that reduction of the Fe(III) salt to an Fe(II) intermediate occurs, followed by the decomposition of the intermediate at high temperature. The formation of an Fe(II) intermediate was indicated by the fact that product separated after a short refluxing time (5 min) instead of 30 min showed no magnetic response and contained FeO, as evidenced by XRD. Furthermore, in the presence of a slight excess of 1-hexadecanethiol, a black powder corresponding to FeS (as characterized by ICP-OES analysis and XRD) could be separated. If Fe(II) (D-gluconate) or Fe(II) acetylacetonate was used, the same product was obtained. No metallic Fe was detected in the final product.

MFe_2O_4 (M = Co, Mn) Nanoparticles. The process described in Scheme 1 can be readily extended to the synthesis of other types of MFe_2O_4 nanoparticles. For example, when Co-(acac)$_2$ was partially substituted for Fe(acac)$_3$ in a 1:2 ratio in the same reaction conditions as in the synthesis of Fe_3O_4, $CoFe_2O_4$ nanoparticles were formed. When Mn(acac)$_2$ was used, $MnFe_2O_4$ nanoparticles were made. ICP-OES elemental analysis indicated that the ratio of Co/Fe and Mn/Fe in both cobalt ferrite and manganese ferrite was retained from the ratio of initial metal precursors, and the final Co/Fe and Mn/Fe compositions could be readily controlled. Figure 7 shows the TEM images of 14 nm $CoFe_2O_4$ nanoparticles and 14 nm $MnFe_2O_4$ nanoparticles made from seed-mediated growth. XRD for both samples are very similar to that of Fe_3O_4, indicating the cubic spinel structure of the particles. At temperatures up to 300 K, 16 nm $CoFe_2O_4$ nanoparticles are ferromagnetic. Figure 8 shows the hysteresis loops of 16 nm $CoFe_2O_4$ nanoparticles measured at both 10 and 300 K. The coercivity of the assembly is about 400 Oe at 300 K, but reaches 20 kOe at 10 K, much larger than that of the 16 nm Fe_3O_4 nanoparticles (450 Oe at 10 K), indicating that the incorporation of the Co cation in the Fe−O matrix greatly increases the magnetic anisotropy of the materials. Such anisotropy enhancement of $CoFe_2O_4$ vs Fe_3O_4 has also been observed in films deposited from aqueous solution.[23] To the contrary, the incorporation of Mn cation in the Fe−O matrix reduces the magnetic anisotropy of the materials,[1a] as the 14 nm $MnFe_2O_4$ nanoparticles shows a coercivity of only 140 Oe at 10 K.

Possible Applications of MFe_2O_4 Nanoparticles. The MFe_2O_4 nanoparticles presented above may have numerous
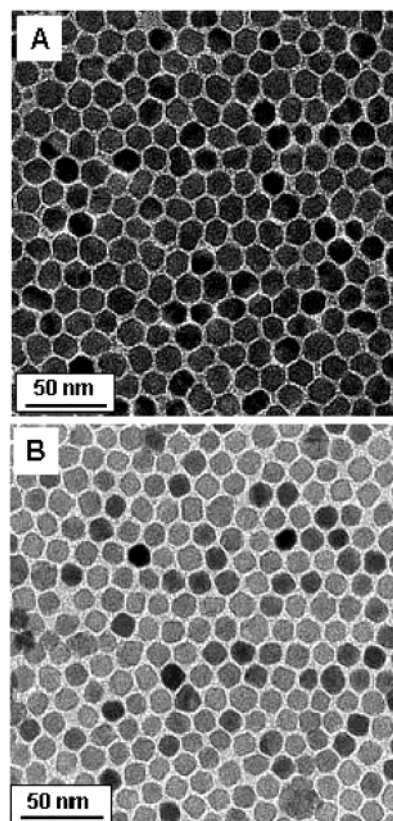
Figure 7. TEM bright field images of (A) 14 nm $CoFe_2O_4$ nanoparticles and (B) 14 nm $MnFe_2O_4$ nanoparticles made from seed-mediated growth and deposited from their hexane dispersion on amorphous carbon-coated copper grid at room temperature.
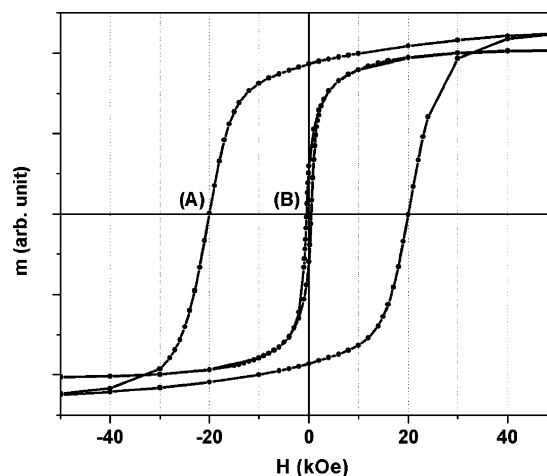
Figure 8. Hysteresis loops of the 16 nm $CoFe_2O_4$ nanoparticle assembly measured at (A) 10 K and (B) 300 K.

applications in magnetic nanodevices and biomedicine, but additional requirements may arise from particular applications. For example, in biomagnetic applications, the superparamagnetic nanoparticles often need to be water-soluble.[3,24] Here we demonstrate briefly that superparamagnetic Fe_3O_4 nanoparticles can be made water-soluble and yield a good magnetic signal that is suitable for spin valve sensor detection.

To make water-soluble iron oxide nanoparticles, we mix hydrophobic nanoparticles with a bipolar molecule, tetramethylammonium 11-aminoundecanoate. Shaking the hexane disper-

(22) Morales, M. P.; Veintemillas-Verdaguer, S.; Montero, M. I.; Serna, C. J.; Roig, A.; Casas, L.; Martinez, B.; Sandiumenge, F. *Chem. Mater.* **1999**, *11*, 3058.

(23) Kim, T. Y.; Lee, M. S.; Kim, Y. I.; Lee, C.-S.; Park, J. C.; Kim, D. *J. Phys. D: Appl. Phys.* **2003**, *36*, 1451.

(24) Fu, L.; Dravid V. P.; Johnson, D. L. *Appl. Surf. Sci.* **2001**, *181*, 173.
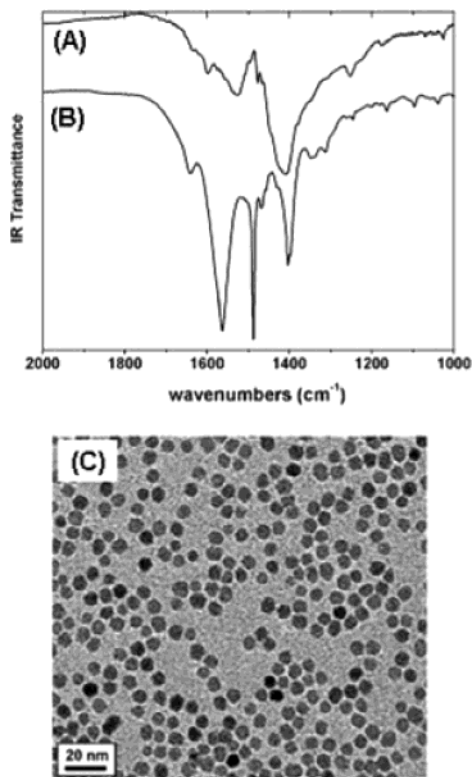
Figure 9. (A) Infrared spectrum of the as-synthesized hydrophobic 6 nm Fe_3O_4 nanoparticles, (B) infrared spectrum of tetramethylammonium 11-aminoundecanoate-coated 6 nm Fe_3O_4 nanoparticles, and (C) TEM bright field image of the 6 nm Fe_3O_4 nanoparticles in (B) deposited from water dispersion on amorphous carbon-coated copper grid.

sion of 6 nm Fe_3O_4 nanoparticles with a suspension of tetramethylammonium 11-aminoundecanoate in dicholoromethane rendered Fe_3O_4 nanoparticles hydrophilic and water-soluble. Figure 9 shows the IR spectra of both the hydrophobic nanoparticles (Figure 9A) and the hydrophilic ones (Figure 9B). The absorptions around 1565 and 1478 cm^{-1} in Figure 9B from the hydrophilic nanoparticles match with the one from free tetramethylammonium 11-aminoundecanoate (1566, 1487 cm^{-1}), indicating the existence of the free $-COO^-$ group in the hydrophilic nanoparticles.[25] Figure 9C is the TEM image of 6 nm Fe_3O_4 nanoparticles from aqueous dispersion. It indicates that nanoparticles in water are well dispersed without any noticeable agglomeration.

Magnetic nanoparticles dispersed in water are superparamagnetic and under a tickling field can yield good magnetic signals that are readily sensed by a spin valve sensor. Such a sensor has been patterned as rectangular strips with a submicron width and a magnetoresistance (MR) ratio of 10% and has shown great potential as a sensitive and efficient detector for biomolecules

labeled by magnetic nanoparticles.[12,26] We have performed several experiments on a monolayer of 16 nm Fe_3O_4 nanoparticles deposited on the 0.3 μm wide spin valve sensors via poly-(ethylenimine)-mediated self-assembly.[27] These submicron spin valve sensors produced signals on the order of 10 μV due to the presence of a layer of Fe_3O_4 nanoparticles. This suggests that these magnetic nanoparticles, if functionalized with single-strand DNA and immobilized on a similarly functionalized spin valve surface via DNA hybridization, could be used as labels for highly sensitive and quantitative DNA detection.

Conclusions

We have reported a convenient organic phase process of making monodisperse MFe_2O_4 nanoparticles through the reaction of metal acetylacetonate and 1,2-hexadecanediol. The diameter of the particles is tunable from 3 to 20 nm by varying reaction conditions or by seed-mediated growth. The process does not require a low-yield fractionation procedure to achieve the desired size distribution and is readily scaled up for mass production. The hydrophobic nanoparticles can be transformed into hydrophilic ones by mixing with bipolar surfactants, allowing preparation of aqueous nanoparticle dispersions. These iron oxide nanoparticles and their aqueous dispersions have great potential in magnetic nanodevice and biomagnetic applications.

Supporting Information Available: Figure S1: Thermal gravimetric analysis (TGA) results for hydrophilic Fe_3O_4 and hydrophobic Fe_3O_4 nanoparticles. This material is available free of charge via the Internet at http://pubs.acs.org.

JA0380852

(25) If the $-COO^-$ attaches to the surface of Fe_3O_4 particles, the IR spectrum will show absorptions in different region and intensity, as the IR spectrum of a model compound ferric stearate exhibits four broad, asymmetric peaks at 1466, 1534, 1589, 1613 cm^{-1}. It should also be noted that whether or not the $-NH_2$ in the 11-aminoundecanoate unit is bound to the particle surface has not been determined. From the IR data, we cannot exclude the presence of the oleate and oleylamine species in the hydrophilic particles. Thermal gravimetric analysis (TGA) (see Supporting Information) of this material shows a sharp mass loss at relatively low temperature (200 °C), but above 300 °C the curve seems similar to that of hydrophobic particles, losing mass between 380 and 440 °C. This seems to suggest that the bipolar surfactant does not displace a significant amount of the original ligands and is loosely bound, forming a bilayer or intercalated layer.
(26) (a) Baselt, D. R.; Lee, G. U.; Natesan, M.; Metzger, S. W.; Sheehan, P. E.; Colton, R. J. *Biosens. Bioelectron.* **1998**, *13*, 731. (b) Edelstein, R. L.; Tamanaha, C. R.; Sheehan, P. E.; Miller, M. M.; Baselt, D. R.; Whitman, L. J.; Colton, R. J. *Biosens. Bioelectron.* **2000**, *14*, 805. (c) Miller, M. M.; Sheehan, P. E.; Edelstein, R. L.; Tamanaha, C. R.; Zhong, L.; Bounnak, S.; Whitman, L. J.; Colton, R. J. *J. Magn. Magn. Mater.* **2001**, *225*, 138.
(27) (a) Sun, S.; Anders, S.; Hamann, H. F.; Thiele, J.-U.; Baglin, J. E. E.; Thomson, T.; Fullerton, E. E.; Murray, C. B.; Terris, B. D. *J. Am. Chem. Soc.* **2002**, *124*, 2884. (b) Sun, S.; Anders, S.; Thomson, T.; Baglin, J. E. E.; Toney, M. F.; Hamann, H. F.; Murray, C. B.; Terris, B. D. *J. Phys. Chem. B* **2003**, *107*, 5419.